Ideal plasma response to vacuum magnetic fields with resonant magnetic perturbations in non-axisymmetric tokamaks

IOP Publishing Plasma Physics and Controlled Fusion
Plasma Phys. Control. Fusion **57** (2015) 104002 (7pp) doi:10.1088/0741-3335/57/10/104002

Ideal plasma response to vacuum magnetic fields with resonant magnetic perturbations in non-axisymmetric tokamaks

Kimin Kim[1,2], J-W Ahn[3], F Scotti[4], J-K Park[1] and J E Menard[1]

[1] Princeton Plasma Physics Laboratory, Princeton, NJ 08543, USA
[2] Korea Advanced Institute of Science and Technology, Daejeon 305-701, Korea
[3] Oak Ridge National Laboratory, Oak Ridge, TN 37831, USA
[4] Lawrence Livermore National Laboratory, Livermore, CA 94551, USA

E-mail: kimk@kaist.ac.kr

Received 31 January 2015, revised 10 June 2015
Accepted for publication 25 June 2015
Published 3 September 2015

Abstract

Ideal plasma shielding and amplification of resonant magnetic perturbations in non-axisymmetric tokamak is presented by field line tracing simulation with full ideal plasma response, compared to measurements of divertor lobe structures. Magnetic field line tracing simulations in NSTX with toroidal non-axisymmetry indicate the ideal plasma response can significantly shield/amplify and phase shift the vacuum resonant magnetic perturbations. Ideal plasma shielding for $n = 3$ mode is found to prevent magnetic islands from opening as consistently shown in the field line connection length profile and magnetic footprints on the divertor target. It is also found that the ideal plasma shielding modifies the degree of stochasticity but does not change the overall helical lobe structures of the vacuum field for $n = 3$. Amplification of vacuum fields by the ideal plasma response is predicted for low toroidal mode $n = 1$, better reproducing measurements of strong striation of the field lines on the divertor plate in NSTX.

Keywords: resonant magnetic perturbation, field line tracing, plasma response

(Some figures may appear in colour only in the online journal)

1. Introduction

The importance of resonant magnetic perturbation (RMP) by externally applied non-axisymmetric magnetic fields has been continuously emphasized for the control of edge localized modes (ELMs) in tokamaks throughout the first demonstration of ELM suppression on DIII-D [1] and the successes in other devices [2–4]. It has been a well-known explanation that the RMP forms stochastic transport layers at the pedestal and enhances particle transport to keep the plasma marginally inside ELM stability boundary. The formation of the stochastic layers by RMP has been well elucidated so far using vacuum field approximation, ignoring plasma response to the non-axisymmetric fields.

Plasmas in tokamaks, however, respond to the applied non-axisymmetric magnetic fields by driving perturbed plasma currents, which induce perturbed magnetic fields to either amplify or shield the applied fields [5–8]. That is, the perturbed magnetic field structure in practice can be significantly changed. The shielding of RMP has been widely studied and understood as plasma flow effects shielding the RMP penetration into plasmas. Much effort has been made to understand such plasma response to internal and/or external magnetic perturbations in tokamaks and helical systems including stellarators [9–13]. There are models describing plasma response, developed to calculate stochastic field structure with or without finite plasma resistivity [14–18], however, the final solution of perturbed equilibria strongly depends on the model used [18]. Work is still underway to achieve a complete solution of the perturbed equilibria including nonideal and nonlinear magnetohydrodynamic (MHD) processes, and the plasma response must be properly considered in the RMP

studies to better understand underlying physics mechanism of stochastic transport and ELM control.

In this paper, we study the stochastic layer structure in the perturbed tokamak using the vacuum field approximation and the perturbed equilibrium with an ideal plasma response. A main focus of this paper is to qualify the stochastic features of the ideal perturbed equilibrium compared to the vacuum field. We use a full ideal plasma response calculation to achieve the total perturbed field for field line tracing simulations, and show the plasma response can significantly modify the characteristics of magnetic field structure in the presence of the non-axisymmetric magnetic fields. It is found that field line tracing simulations employing full ideal plasma response may better explain the diverter footprint observations for low n experiments like $n = 1$.

2. Field line tracing simulation

The field line tracing simulation is a well-known tool to study the stochastic magnetic field structure in the non-axisymmetric magnetic perturbations. It is useful to display and investigate the formation and modification of stochastic layers by the non-axisymmetric perturbations [4, 19–21]. A new field line tracing routine is used in this study, which has been implemented in the POCA code [22–24] by solving a set of magnetic differential equations

$$\frac{\partial R}{\partial \phi} = \frac{RB_R}{B_\phi}, \qquad \frac{\partial Z}{\partial \phi} = \frac{RB_Z}{B_\phi}.$$

Here, (B_R, B_Z, B_ϕ) are the magnetic field strength on the cylindrical coordinates (R, Z, ϕ). The field line tracing routine, called POCA-FLT, solves the magnetic differential equations in the realistic tokamak geometry including the plasma facing components such as divertor, limiter and wall structures, as well as the separatrix. This simulation provides various output information for a given non-axisymmetric magnetic field, such as the field line connection length, the field line loss fraction, the Poincare map at the prescribed toroidal angle, and the magnetic footprint on the divertor plate covering the full toroidal angle. The POCA-FLT code is similar to other existing field line tracing codes in general. However, it has convenient features designed to study the physics of plasma response through a coupling to the ideal perturbed equilibrium code, IPEC [25]. The IPEC code provides POCA-FLT the perturbed magnetic field information calculated with the vacuum field approximation and the ideal plasma response.

One feature is that POCA-FLT can separately track the perturbed magnetic field lines produced by intrinsic error fields in NSTX, which are extracted by IPEC run. The error field effects can be independently studied without non-axisymmetric field coils. Typical simulation results are shown in figure 1, where the magnetic footprints on the divertor target are drawn by contour plots of field line connection length for an error field correction discharge in NSTX. The field line connection length is calculated by tracking a magnetic field line for 200 toroidal turns in co- and counter-Ip directions until the field line touches plasma facing components. This is a useful parameter that can be compared with camera images on the diverter (figures 4 and 7) since large connection length implies the field lines stay in the hot plasma core for longer time to carry high heat fluxes [26]. Figure 1(a) is the footprint by intrinsic $n = 3$ error fields from PF5 coils [27, 28] without applying the non-axisymmetric coil currents, and figure 1(b) is the one by combined fields of the PF5 error fields and correction fields supplied by the midplane error field correction coils in NSTX. Here, n is the toroidal mode number. As seen in the figure, the PF5 intrinsic error fields create helical lobe structures represented by typical striation patterns of the $n = 3$ mode. However, figure 1(b) indicates that the helical lobes disappear when the correction fields are applied by the error field correction coils, as achieved in the experiment. The separate treatment of the error fields would be useful to investigate observations of the lobes even without midplane coil currents in several NSTX discharges.

Another feature is that the POCA-FLT simulation can fully take into account the ideal plasma response that shields the normal resonant field at the rational surfaces [29]. Such a capability is important since the plasma response plays a crucial role in forming and altering the stochastic layers as reported in [30, 31], where a helical current sheets model aligned with the external field was applied to represent the screening of the resonant magnetic perturbations. The POCA-FLT performs the field line tracing in a similar manner but employs a full ideal plasma response calculation by IPEC.

3. Shielding of vacuum field by ideal plasma response

One can find that the stochasticity is significantly modified by the ideal plasma shielding in the Poincare maps in figure 2, where $n = 3$ non-axisymmetric field was applied using the midplane coils in NSTX. The same colors in the contour indicate the same initial flux surfaces where tracking of the field line begins (i.e. core: blue, edge: red). There is one free parameter $\psi_{\rm lim}$, the computational boundary of ideal plasma in the simulation; the IPEC code computes the perturbed equilibria with the ideal plasma up to a certain normalized poloidal flux $\psi_{\rm lim}$. The volume outside $\psi_{\rm lim}$ is treated as vacuum, but overall force balance is still maintained.

Figure 2(a) shows a Poincare map with typical $n = 3$ helical lobe structure generated by the midplane coils in NSTX using the vacuum fields. The splitting of the field lines towards the divertor plate is consistent with an observation of the split striking points in NSTX [21]. Islands open on the rational flux surfaces by the resonant field components, and overlap to form the stochastic layers in the whole region. On the other hand, the stochasticity is largely changed by inclusion of the ideal plasma response with $\psi_{\rm lim} = 0.97$ as shown in figure 2(b). The stochastic layers formed inside $\psi_{\rm lim}$ by the vacuum fields disappear due to shielding of the resonant field components. Magnetic islands are not opened in the inner region but altered to make a wobble-like structure on the flux surfaces, which is identical to the perturbed flux surface. However, islands reopen due to unshielded resonant

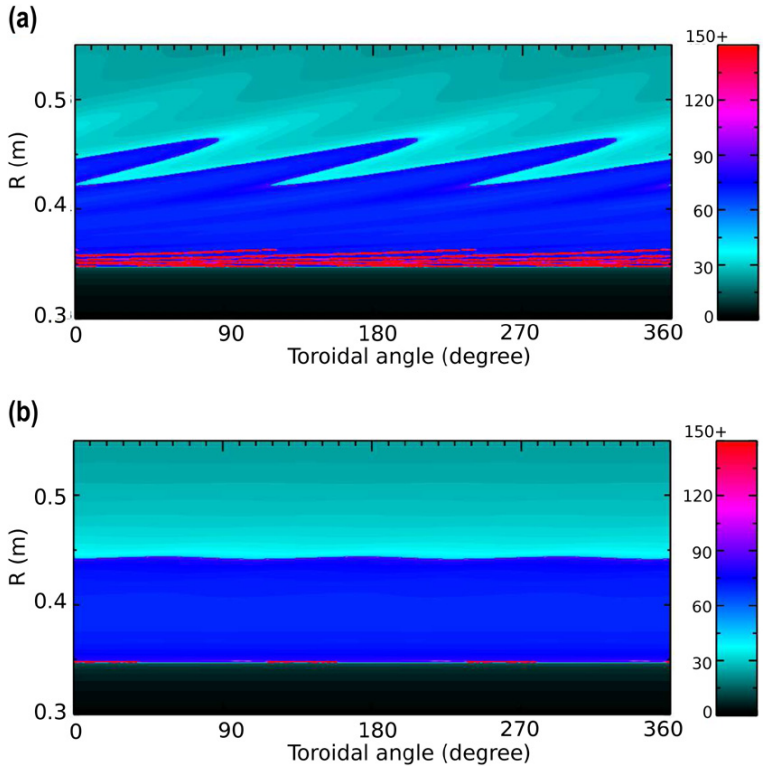

Figure 1. Contour plot of field line connection length for (a) $n = 3$ PF5 error fields and (b) correction of the error fields using error field correction coils in NSTX. These contours indicate (a) striation of the field lines by the intrinsic error fields and (b) correction of the error fields.

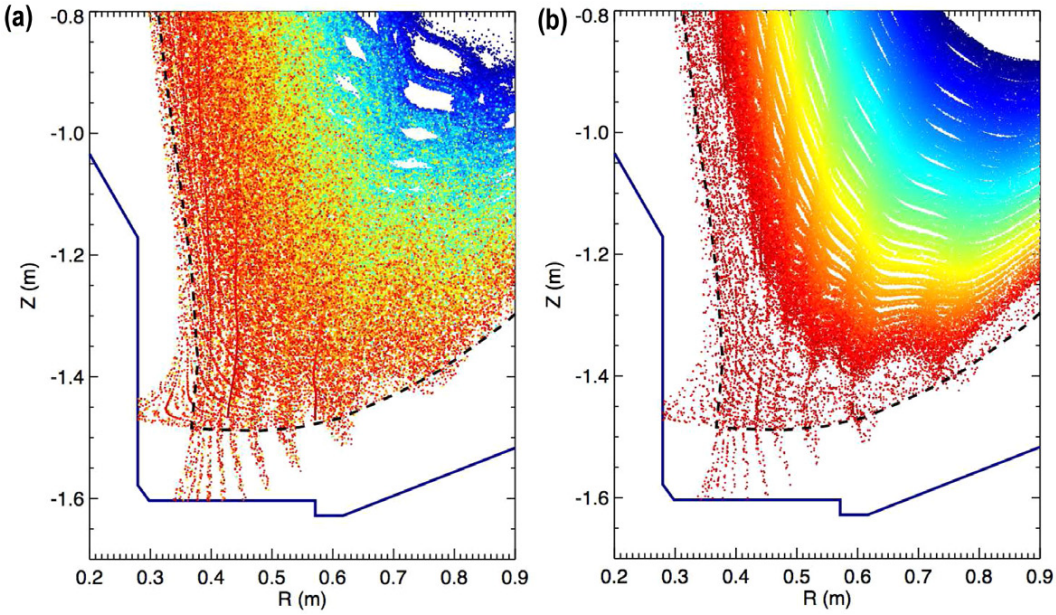

Figure 2. Poincare map of the magnetic field lines with (a) vacuum approximation and (b) ideal plasma response computed by IPEC with $\psi_{\mathrm{lim}} = 0.97$. Broken line indicates the separatrix of the axisymmetric equilibrium.

components in the vacuum region outside ψ_{lim}, thus stochasticity arises again to create almost identical helical lobes to the ones predicted by the vacuum fields. It should be noted that the wobble-like structure in figure 2(b) is due to the current sheet at the rational surfaces driven by the ideal plasma response in this simulation. Such shielding effects are not

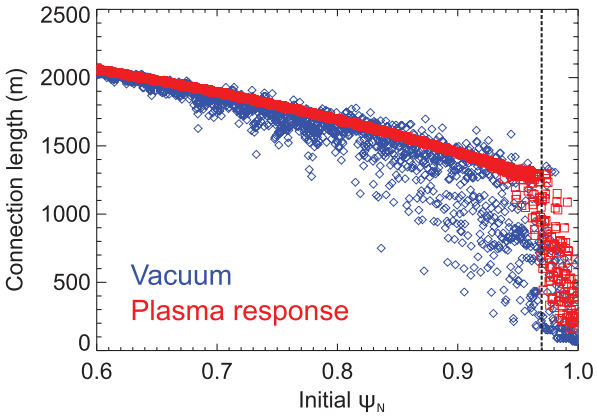

Figure 3. Field line connection length profile with the vacuum field approximation and the ideal plasma response as a function of initial ψ_N. Vertical broken line indicates the boundary of the ideal plasma at $\psi_{lim} = 0.97$.

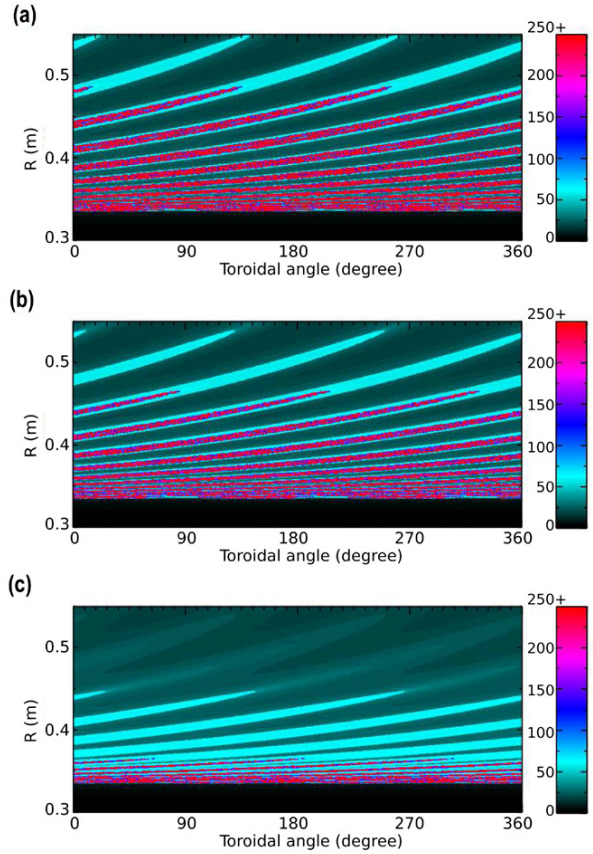

Figure 4. Contour plot of field line connection length by $n = 3$ non-axisymmetric field with (a) the vacuum field approximation and the ideal plasma response of (b) $\psi_{lim} = 0.97$, and (c) $\psi_{lim} = 0.99$. Increasing ψ_{lim} leads to weaker striations.

guaranteed in the presence of nonideal plasma response with finite resistivity.

One can see the modification of stochasticity more clearly in figure 3, where the field line connection length profiles are plotted for the same case in figure 2. Note the x-axis is not the radial position of the Poincare map in figure 2 but

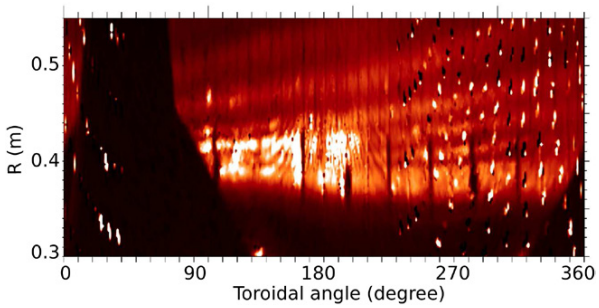

Figure 5. Wide angle visible camera image to be compared with figure 4.

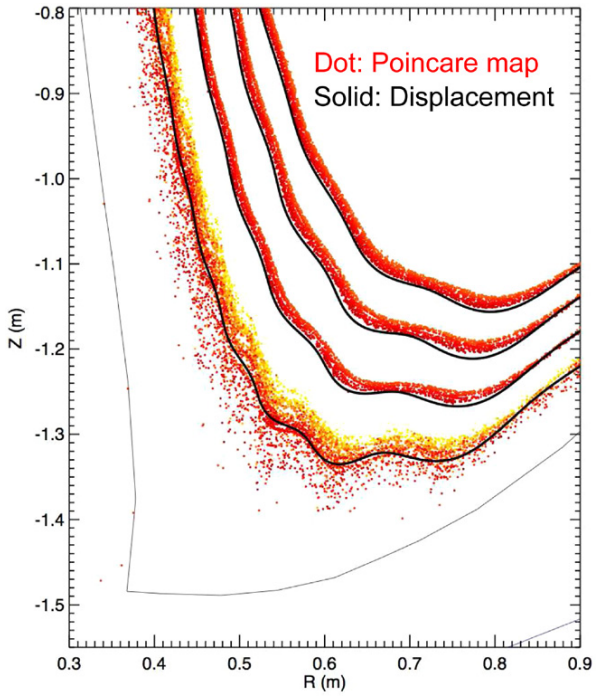

Figure 6. Poincare plot of the field line tracing simulation including the ideal plasma response ($\psi_{lim} = 0.97$), compared to the perturbed flux surface constructed with ideal plasma displacements computed by IPEC.

the initial normalized poloidal flux where tracing the field lines begins. The connection length in the vacuum field is found to be shorter than the ideal plasma response case on the rational surfaces because island overlapping moves out the field line fast. Therefore, the connection length profile appears stochastic as well. However, field lines are well-confined by the ideal plasma shielding, thus the connection length becomes an almost continuous function inside ψ_{lim}. The ideal plasma shielding causes an amplification of plasma currents and thereby amplification of the perturbed field outside the ideal plasma boundary to maintain the force balance. This is consistent with the increased connection length outside the boundary. It should be noted that a slight inside of ψ_{lim} in the ideal case is stochastic, however, it does not mean the ideal plasma response breaks the magnetic flux conservation. As noted earlier, since the x-axis of figure 3 is the initial flux

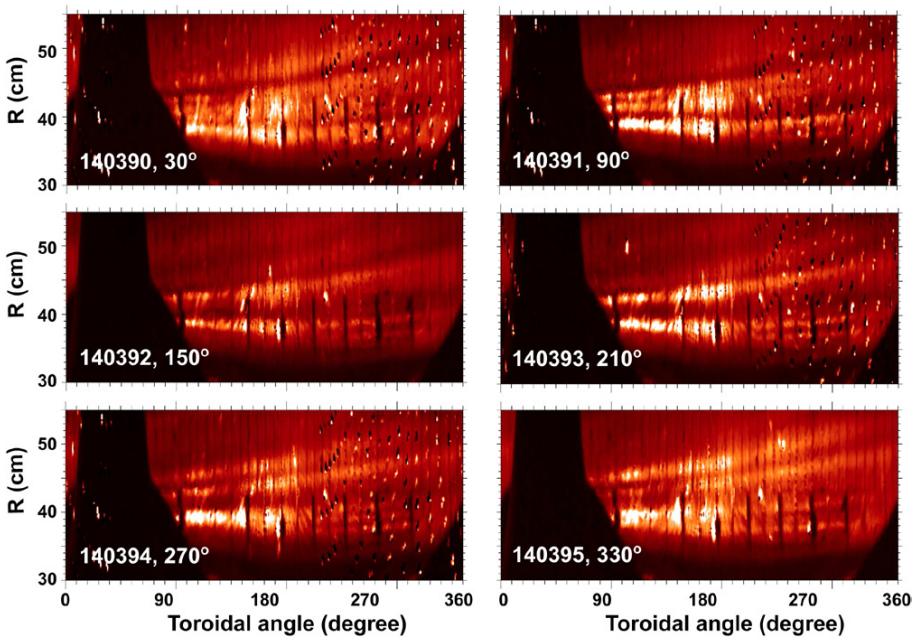

Figure 7. Wide angle camera images of divertor lobe structure for experiments scanning footprint with $n = 1$ phase angle. Strong and static striations were observed regardless of the coil phase angle.

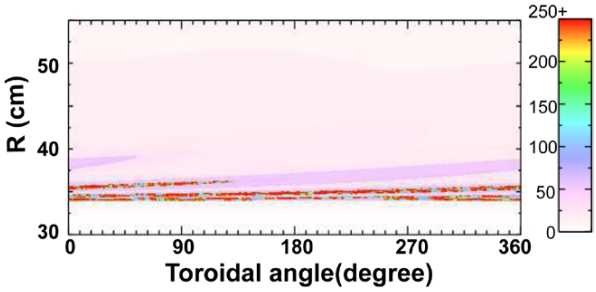

Figure 8. Divertor footprint by typical $n = 1$ perturbation, obtained from connection length in field line tracing simulation using vacuum fields. Much weaker striation than measurement was computed.

surface for the field line tracing, the stochastic layer inside of $\psi_{\rm lim}$ indicates flux lines on those surfaces can be connected to vacuum layer due to the wobble-like structure in the vicinity of the ideal plasma boundary as shown in figures 2(b) and 6. This mixes the ideal plasma and the vacuum layers, and self-consistent models will be required in the future to better understand such complicated mixed structures.

The effects of the ideal boundary $\psi_{\rm lim}$ can be quantitatively examined with magnetic footprints. Figures 4(a)–(c) are contour plots of field line connection length for the vacuum and the ideal perturbed equilibrium with $\psi_{\rm lim} = 0.97$ and 0.99 for the same case in figure 2. The vacuum case in figure 4(a) presents striations of field lines on the target produced by $n = 3$ vacuum field, showing consistent patterns with the observation by a wide angle visible camera in figure 5 [32], where neutral lithium emission is used to image striations on the lower divertor plasma facing components [33]. Figure 4(b) with $\psi_{\rm lim} = 0.97$ shows similar but weaker striations due to the shielding of resonant field components. Pushing the ideal plasma region to $\psi_{\rm lim} = 0.99$ makes the footprints even weaker due to stronger shielding effects in figure 4(c). The simulation results indicate the plasma may respond to the externally applied field to modify the stochasticity in the non-axisymmetric magnetic perturbations. A quantitative comparison between extended numerical models and divertor heat flux measurement will be further required for validating plasma response models and understanding underlying physics.

Defining the perturbed flux surfaces of the perturbed equilibria is one issue to be resolved. The perturbed flux surface can be established by normal plasma displacement in the ideal MHD, while it can be also obtained from the Poincare map in the field line tracing or contours of the perturbed electron temperature in the resistive approach [18]. Figure 6 is a direct comparison of the perturbed flux surfaces between the Poincare map of field lines with ideal plasma response and the normal displacement computed by IPEC. The solid curves in the figure are the superposition of normal displacements on the axisymmetric flux surfaces. It is found that the perturbed flux surfaces from the ideal displacements agree with the wobble-like structures of Poincare plot in the ideal plasma region, as pronounced by a relation between the perturbed magnetic field and the displacement $\vec{\xi}$ by $\delta\vec{B} = \vec{\nabla} \times (\vec{\xi} \times \vec{B}_0)$ in the ideal MHD theory. However, the magnetic field lines are stochastic around the ideal plasma boundary, so the perturbed flux surfaces cannot be well defined from the vacuum approximation.

4. Amplification of vacuum field by ideal plasma response

Plasmas can respond to the applied non-axisymmetric fields to amplify and/or phase shift the perturbations [29]. The

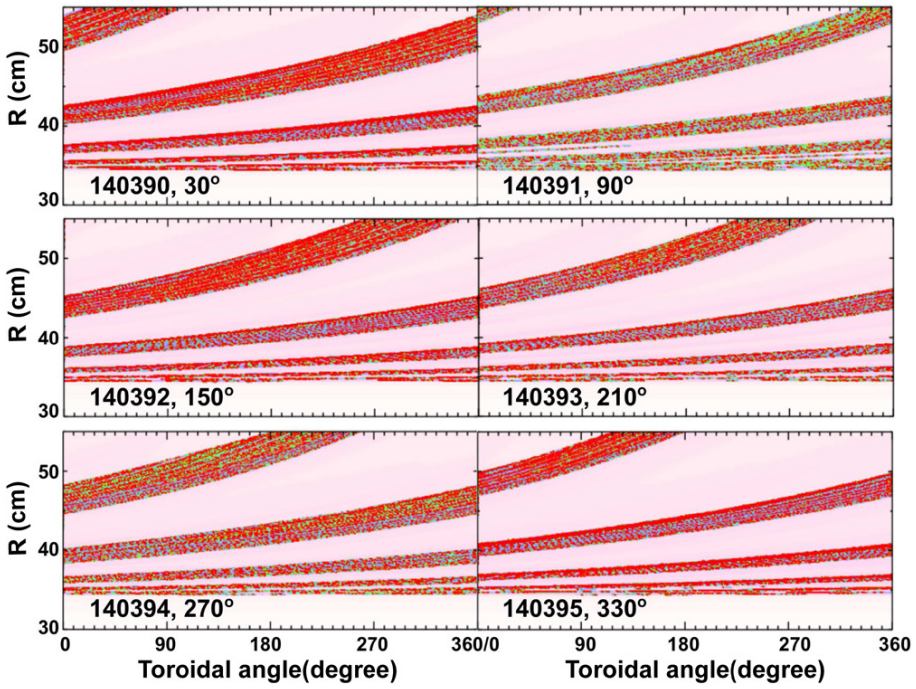

Figure 9. Divertor footprints by $n = 1$ fields for each coil phase angle, calculated by field line tracing simulations including ideal plasma response. Strong striations were reproduced due to amplification of vacuum fields, giving much better agreement with measurements.

midplane non-axisymmetric field coils in NSTX are capable of applying the $n = 1$ perturbations in the six phase angle, providing toroidally phase shifted $n = 1$ fields depending on the angle. The modification of the magnetic field line structure by the $n = 1$ magnetic perturbations has been investigated using a series of discharges measuring helical lobe structure by the $n = 1$ fields in the six coil phases. The wide angle visible camera has been used to image the footprints of magnetic field lines on the divertor plate for each discharge, which are summarized in figure 7. The general expectation was that the phase angle shift of the coils will produce toroidally phase-shifted striation patterns corresponding to the shifted $n = 1$ field. However, as shown in the figure 7, two interesting points were observed in the experiments; first, strong striations in the helical lobe structure are captured in every discharge. Second, measured lobe structures do not show a clear phase-shift of the patterns in spite of the phase angle shift between the discharges.

Vacuum field line tracing simulations have been attempted to understand the experimental observation, and it was found that the vacuum field approximation ignoring the plasma response was not valid for these experiments. The vacuum field line tracing simulation result for the $n = 1, 30$ degree case (140390) is shown in figure 8 as an example. It is clear that experimentally measured strong striation of the footprint pattern cannot be achieved by the vacuum fields even though every possible field component of NSTX was included in the calculation (e.g. $n = 1$ and $n = 3$ components from midplane, PF5, and TF coils). On the other hand, clear toroidal rotation of the footprint patterns due to the phase angle shift was obtained in the calculations (not shown). Unlike the $n = 3$ cases, vacuum field line tracing was not able to reproduce and explain neither of strong striation and static patterns presented in the wide angle camera images in figure 7.

It is implied that the vacuum fields should be amplified and phase shifted to narrow the discrepancies between observations and calculations and the plasma response may be responsible for the field modification. We consider the ideal plasma response calculation and equilibrium reconstruction using kinetic EFIT. The kinetic EFIT including steep pedestal structure and strong contribution of bootstrap current was utilized for IPEC and POCA-FLT computations, where edge safety factor and its shear profile strongly impacted on both axisymmetric and non-axisymmetric equilibriums. Calculation results combining the ideal plasma and kinetic EFIT are presented in figure 9. They indicate that modification of the applied non-axisymmetric fields by ideal plasma response dramatically amplified the amplitudes of vacuum $n = 1$ fields and produced more consistent diverter footprints to the camera image. The ideal plasma response was found to significantly modify the envelope of lobes of vacuum fields unlike $n = 3$ cases, therefore, striation patterns were also significantly changed from the ones by vacuum fields. Overall field line tracing simulations including the ideal plasma response provide much better agreement with the camera images.

One can notice that some local discrepancies between measurements and calculations still remain. Measurements show that almost stationary footprint patterns were created in the discharges despite the phase angle change, even though rotation of vacuum $n = 1$ fields may have to produce

toroidally rotating footprint patterns. Field line tracing simulations with ideal plasma response present partially stationary and partially rotating footprint patterns, as presented by discontinuities of lobe structures between discharges in the simulation. Footprints by externally applied $n = 1$ fields rotate toroidally, however, the amplification of intrinsic error fields by the ideal plasma response included in the simulations for figure 9 compensates such rotating effects and produces partially stationary striation patterns.

Note strong amplifications of $n = 1$ fields cause a significant mixing of the ideal plasma and the vacuum layers as stated in section 3. They produce a significant amount of new field line connections from edge to divertor plates that are not captured in the vacuum field line tracing, and modify footprint shapes on the divertor plates. The inclusion of other error field sources makes the pattern by the ideal plasma response look more different from vacuum field case. They can look even more different especially when the field sources are complicated across intrinsic and applied components with different toroidal modes.

More evidence will be required to confirm that the ideal plasma response is solely responsible for the divertor footprints in the $n = 1$ magnetic perturbations on NSTX. Instead, it would be possible to argue that the ideal plasma response can play significant roles in modifying the magnetic field structure, which better explains the $n = 1$ experiments of NSTX. It is also clear that self-consistent non-axisymmetric equilibria is necessary for better understanding of observations. Since plasmas in reality are non-ideal and lie somewhere between ideal and vacuum regimes, ideal or vacuum model can be a good approximation depending on the discharges. However, more advanced plasma response model must be taken into account to achieve full physical mechanism of the non-axisymmetric perturbed equilibria in tokamaks. An ideal plasma response model can be one approach as shown in this paper, however, robust and complete models including non-ideal effects should be studied and cross-benchmarked.

5. Conclusions

Field line tracing simulations using POCA-FLT code show that ideal plasma response can shield or amplify the externally applied vacuum non-axisymmetric magnetic fields. Simulation results found the ideal plasma response shielding of $n = 3$ vacuum fields and amplification of $n = 1$ fields, implying vacuum fields can be significantly modified in amplitude and phase by the plasma response. The impacts of plasma response will be even more complicated in the presence of non-ideal and nonlinear MHD processes. The inclusion of such rich physics remains a future work. It is clearly indicated in this study that the plasma response must be taken into account in the non-axisymmetric tokamak physics study to better understand the stochastic plasma transport and ELM suppression, which eventually will require a self-consistent perturbed equilibria.

Acknowledgments

This work was supported by DOE Contract DE-AC02-09CH11466 (PPPL) and DE-AC52-07NA27344 (LLNL). Part of the work was supported by the National Research Foundation of Korea (NRF) funded by the Ministry of Science, ICT and Future Planning (NRF-2014M1A7A1A03045092).

References

[1] Evans T E *et al* 2004 *Phys. Rev. Lett.* **92** 235003
[2] Suttrop W *et al* 2011 *Phys. Rev. Lett.* **106** 225004
[3] Jeon Y M *et al* 2012 *Phys. Rev. Lett.* **109** 035004
[4] Kirk A, Harrison J, Liu Y, Nardon E, Chapman I T, Denner P and the MAST Team 2012 *Phys. Rev. Lett.* **108** 255003
[5] Boozer A H 2001 *Phys. Rev. Lett.* **86** 5059
[6] Boozer A H and Nührenberg C 2006 *Phys. Plasmas* **13** 102501
[7] Lanctot M J *et al* 2010 *Phys. Plasmas* **17** 030701
[8] Chu M S *et al* 2011 *Nucl. Fusion* **51** 073036
[9] Fitzpatrick R 1993 *Nucl. Fusion* **33** 1049
[10] Bécoulet M *et al* 2009 *Nucl. Fusion* **49** 085011
[11] Narushima Y *et al* 2011 *Nucl. Fusion* **51** 083030
[12] Hegna C C 2011 *Nucl. Fusion* **51** 113017
[13] Nishimura S, Toda S, Yagi M and Narushima Y 2012 *Phys. Plasmas* **19** 122510
[14] Boozer A H 2006 *Phys. Plasmas* **13** 044501
[15] Park J-K, Schaffer M J, Menard J E and Boozer A H 2007 *Phys. Rev. Lett.* **99** 195003
[16] Liu Y, Kirk A, Gribov Y, Gryaznevich M P, Hender T C and Nardon E 2011 *Nucl. Fusion* **51** 083002
[17] Ferraro N M, Evans T E, Lao L L, Moyer R A, Nazikian R, Orlov D M, Shafer M W, Unterberg E A, Wade M R and Wingen A 2013 *Nucl. Fusion* **53** 073042
[18] Turnbull A D *et al* 2013 *Phys. Plasmas* **20** 056114
[19] Evans T E, Moyer R A and Monat P 2002 *Phys. Plasmas.* **9** 4957
[20] Jakubowski M W *et al* 2009 *Nucl. Fusion* **49** 095013
[21] Ahn J-W, Maingi R, Canik J M, McLean A G, Lore J D, Park J-K, Soukhanovskii V A, Gray T K and Roquemore A L 2011 *Phys. Plasmas* **18** 056108
[22] Kim K, Park J-K, Kramer G J and Boozer A H 2012 *Phys. Plasmas* **19** 082503
[23] Kim K, Park J-K and Boozer A H 2013 *Phys. Rev. Lett.* **110** 185004
[24] Kim K, Park J-K, Boozer A H, Menard J E, Gerhardt S P, Logan N C, Wang Z R, Kramer G J, Burrell K H and Garofalo A M 2014 *Nucl. Fusion* **54** 073014
[25] Park J-K, Boozer A H and Glasser A H 2007 *Phys. Plasmas* **14** 052110
[26] Wingen A, Evans T E and Spatschek K H 2009 *Phys. Plasmas* **16** 042504
[27] Gerhardt S P, Menard J E, Park J-K, Bell R, Gates D A, Le Blanc B P, Sabbagh S A and Yuh H 2010 *Plasma Phys. Control. Fusion* **52** 104003
[28] Menard J E *et al* 2010 *Nucl. Fusion* **50** 045008
[29] Park J-K, Boozer A H, Menard J E, Gerhardt S P and Sabbagh S A 2009 *Phys. Plasmas* **16** 082512
[30] Cahyna P, Nardon E and JET EFDA Contributors 2011 *J. Nucl. Mater.* **415** S927
[31] Frerichs H, Reiter D, Schmitz O, Cahyna P, Evans T E, Feng Y and Nardon E 2012 *Phys. Plasmas* **19** 052507
[32] Ahn J-W *et al* 2014 *Plasma Phys. Control. Fusion* **56** 015005
[33] Scotti F, Roquemore A and Soukhanovskii V A 2012 *Rev. Sci. Instrum.* **83** 10E532